World Conference on Timber Engineering Oslo 2023

EXPERIMENTAL AND FINITE ELEMENT MODELLING (FEM) OF TIMBER-TIMBER COMPOSITE (TTC) UNDER HOGGING MOMENT

Mahmoud Wajdi Hammad[1], Hamid R ValiPour[2]

ABSTRACT: This study aims to investigate the structural behaviour of timber-timber composite (TTC) systems subject to hogging moment. A total of thirty-one TTC and six bare timber beam-to-column subassemblies (including fourteen replicates) were fabricated and tested to failure under hogging moment. The TTC beams were fabricated by connecting a cross laminated timber (CLT) slab to the top edge of a pair of laminated veneer lumber (LVL) or glued laminated timber (GLT) beams/joists. The effect of the CLT slab thickness, width, and orientation (i.e., loaded lengthwise or crosswise), column penetration in the CLT slab, bending moment to shear force ratio (span length), degree of shear interaction between the slabs and beams (controlled by the size of the shear connectors), and type of beams (LVL or GLT) on the structural performance of the TTC subassemblies were investigated experimentally. In addition, an analytical model was adopted for composite Timoshenko beams and modified to predict the stiffness and load carrying capacity of the TTC beams under hogging moment. Furthermore, 3-Dimentional Finite Element Models (FEM) have been developed and analysed for TTC structures subjected to hogging bending moments using ABAQUS.

KEYWORDS: Hogging moment, Timber-timber composite (TTC), Finite Element Modelling (FEM).

1 INTRODUCTION

Since sustainability in construction has become a major headline, the popularity of timber structures has grown significantly. The advancement in the manufacturing and treatment of large engineered wood panels (EWPs) such as cross laminated timber (CLT), glued laminated timber (GLT) and laminated veneer lumber (LVL) with improved durability, dimensional stability and resistance to variable environmental conditions has made it conceivable to plan and construct massive timber structures with performance on par with conventional steel and concrete structures, but with less detrimental impact on the environment [2, 3].

The application of lightweight TTC (i.e., LVL-CLT or GLT-CLT) floors, which are easy to assemble and conducive to prefabrication, seems to be a promising solution for the development of hybrid frames with continuous timber beams/slabs that can cover long spans with fewer columns or load bearing walls. Structural behaviour of timer composite floors (e.g., TTC and TCC) subjected to hogging bending moment remains largely unexplored. Preserving the continuity of CLT slabs and LVL/GLT beams across the columns can reduce the mid-span deflection, which is a major governing factor in designing the long-span TTC floors under service conditions. However, benchmark experimental data required for the accurate evaluation of the failure modes, stiffness, ductility, and load carrying capacity of continuous TTC beams (to column connection) under hogging moment are not available in the literature.

Thus, experiments were conducted to comprehensively study the structural behaviour of CLT-LVL and CLT-GLT composite beams subjected to hogging (negative) moment over the beam-to-column connection zone. In total, thirty-seven TTC and bare timber beam-to-column subassemblies were fabricated and tested under hogging moments.

Furthermore, in the 3-Dimentional Finite Element Models developed, nonlinear behaviour of the Engineered Wood Products (EWPs) such as Cross Laminated Timber (CLT), Laminated Veneer Lumber (LVL) and Glued Laminated Timber (GLT) were defined in a UMAT code using continuum damage mechanics modified by Gharib et al [4]. CLT was modelled using the layer wise approach, assigning parallel and perpendicular to the grain, which will be further discussed in this chapter. Meanwhile, the veneers and the lumber in the LVL and GLT were ignored respectively in ABAQUS, having LVL and GLT

[1] University of New South Wales (UNSW) Sydney, School of Civil and Environmental Engineering, mahmoud.hammad@unsw.edu.au
[2] University of New South Wales (UNSW) Sydney, School of Civil and Environmental Engineering

https://doi.org/10.52202/069179-0008

modelled as a single piece of timber. Steel was modelled using the standard user materials defined in ABAQUS.

The EC5 model is only applicable for timber composite beams/floors under sagging moments and hence there is a need for simple analytical model (like gamma-method) that can be used for stiffness and strength evaluation of timber composite subjected to hogging.

2 MATERIAL TESTING

2.1 ENGINEERED WOOD PRODUCTS (EWP)

The characteristic strength and mean elastic modulus values for C24(CLT), GLT(GL17) and LVL were taken from AS1720.1 [5] and the manufacturer's catalogue, respectively. Moreover, 4-point bending tests on 60 mm and 100 mm thick CLT panels (five identical strips of each thickness) were performed according to BS EN408 [6] to determine the mean global elastic modulus $E_{m,g}$ and bending strength f_b of the CLT panels. The mean global elastic moduli of the 60 mm and 100 mm thick CLT panels (lengthwise) were $E_{m,g}$= 11.3 GPa (CoV = 7.7%) and 9.7 GPa (CoV = 7.6%), respectively. The mean bending strength of the 60 mm and 100 mm thick CLT panels (lengthwise) were f_b = 37.5 MPa (CoV = 13.4%) and 31.9 MPa (CoV = 8.8%), respectively. The glulam (GL13) and LVL beams were manufactured from Radiata Pine in accordance with AS/NZS1328.1 [7] and AS4357.0 [8] requirements, respectively. The characteristic strength and mean elastic modulus of the GL13 and LVL respectively taken from AS1720.1 [5] and the manufacturer's catalogue are given in Table 3 1. The moisture content (MC) of the LVL and GL13 beams were measured by oven-dry method of AS/NZS 1080.1 [9]. The mean MC (obtained from five samples) of the LVL and GL13 are provided in **Table 1** and
Table 2. Bending tests were performed on three 85×336 mm GLT beams and the mean bending strength of GLT beams from the tests was $f_{b,mean}$= 49 MPa (CoV= 9%). The mean bending strength of the GL13 closely correlate with the mean bending strength of 45 MPa obtained from the samples taken from six Australian manufacturers of the glulam [10].

The mean bending strength of 200 mm deep LVL beams was $f_{b,mean}$= 66.5 MPa and it was obtained from the bending tests performed on two pairs of 3.0 m long bare LVL (200 mm deep) beam subassemblies. A size effect strength reduction factor of was considered according to the manufacturer's catalogue and the bending strength of 400 mm deep LVL beams was estimated to be $f_{b,mean}$= 59.7 MPa.

Table 1: *mean elastic modulus of C24 timber (used in manufacturing CLT panels), GLT and LVL beams.*

Timber type	Compressive strength (MPa)		Elastic moduli ‖ (GPa)	Shear moduli (GPa)	Moisture content (%)
	‖ to grain	⊥ to grain			
C24	21	2.5	11.0	0.69	11.6
GLT (GL17)	33	---	16.7	1.11	13.1
LVL	42	12	13.2	0.66	8.6

Table 2: *Characteristic strength (# Flexural strength for 200 mm deep LVL joists)*

Timber type	Bending strength (MPa)	Tensile strength (MPa)	Shear strength (MPa)
C24	24	14	4.0
GLT (GL17)	40	20	4.2
LVL	45#	30	4.6

2.2 DIGITAL IMAGE CORRELATION (DIC)

A digital image correlation (DIC) system was used during the bending tests on LVL (200 mm) beams to capture the strain field over the depth of the beams and accordingly establish the flexural strength and its corresponding strain. The contours of longitudinal strains ε_{xx} and the ε_{xx} strains at three points (i.e., farthest bottom, and top fibre and mid height of LVL) captured by the DIC are shown in Figure 3 1. At the peak load, the max. tensile strain (averaged at the farthest bottom fibre point P1) of the LVL was ε_{xx}=((0.00574+0.0058))/2=0.00577 (**Figure 1**). If a linear elastic behaviour for LVL is assumed, the tensile strength of the 200 mm deep LVL can be estimated from σ_{xx} = 0.00577×E = 0.00577×13200 = 76.2 MPa that confirms the bending strength of LVL.

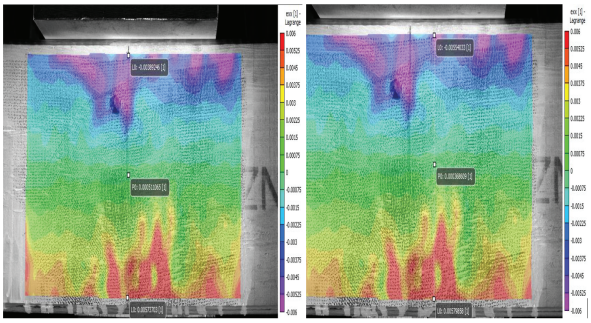

Figure 1: *Contours of ε_{xx} strains (DIC) at failure load of a bare LVL (200 mm) subassembly.*

https://doi.org/10.52202/069179-0008

2.3 SCREWS AND EPOXY (ADHESIVE)

Coach screws (KOP) 8 mm or 12 mm in nominal diameters with hexagonal heads manufactured in accordance with EN 14592 [11] were used as shear connectors in the TTC specimens. The KOP 8 mm screws were 160-200 mm, and the 12 mm screws were 160-220 mm in length **Figure 2**a [12]. The yield bending moment M y of 8 mm and 12 mm coach screws (i.e., KOP8 and KOP12) were obtained from 3-point bending tests in accordance with AS/NZS ISO 10984.1 [13], known as Method B. In total, five screws of each size were tested under 3-point bending with the screws spanning over 132 mm distance between the supports (**Figure 2**a) that satisfies the minimum span requirement of 11d and a minimum overhang of 2d as per AS/NZS ISO 10984.1 [13]. The sample load vs mid-span displacement obtained from the 3-point bending tests on KOP8 screws are plotted in **Figure 2**b. The intersection between the straight line offset 0.05d from the linear part of the graphs and the load-mid span displacement diagram is taken as the yield load F_y. The yield bending moment My of the coach screws was obtained from $My = F_y\, l / 4$, with l = 132 mm being the span length (**Figure 2**a). The mean yield bending moment of the KOP8 and KOP12 screws were My = 15.2 kNm (CoV = 10.6%) and 79.8 kNm (CoV = 9.5%), respectively. The yield strength σ_y of the screws was back calculated from the yield bending moment My, using $\sigma_y = M_y/S$, where S is the plastic section modulus. The plastic section modulus was calculated from $S = (1.1d_{in})3/6$, where d_{in} is diameter of the screw's cross-section excluding the threads and for KOP8 and KOP12 taken as 5.6 mm and 9 mm, respectively. The estimated mean yield strength of the KOP8 and KOP12 screws was σ_y = 442 MPa.

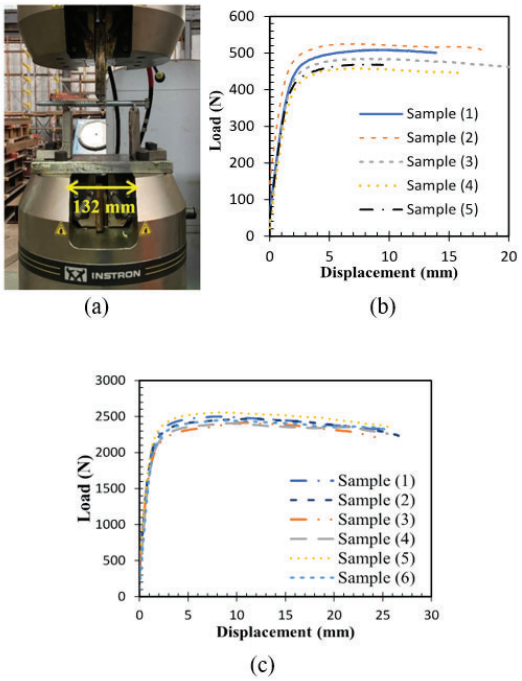

Figure 2: *(a) 3-point bending test of lag screws, and load vs mid span displacement of (b) KOP8, (c) KOP12 from 3-point bending.*

3 TTC SUBJECTED TO HOGGING MOMENT [1]

3.1 LOADING PROCEDURES

All the tests were performed according to the EN 26891 [14] loading protocol. All the specimens were loaded up to $0.4F_{est}$ over 2 minutes, then the load was kept constant for 30 seconds before the specimens were unloaded to $0.1F_{est}$ over 1.5 minutes (Figure 3a). At the end of the unloading stage, the load was kept at $0.1F_{est}$ for 30 seconds, before the specimen was reloaded to failure. The loading-unloading-reloading protocol of EN 26891 [14] was followed to eliminate (or minimise) the possible effects of internal friction between the CLT slab and LVL/GLT or test setup looseness on the structural behaviour of the specimens. The test was stopped once the applied (displacement-controlled) load dropped to 70% of the peak load (F_{max}), and accordingly the failure load was taken as the post-peak load corresponding to $0.7F_{max}$.

https://doi.org/10.52202/069179-0008

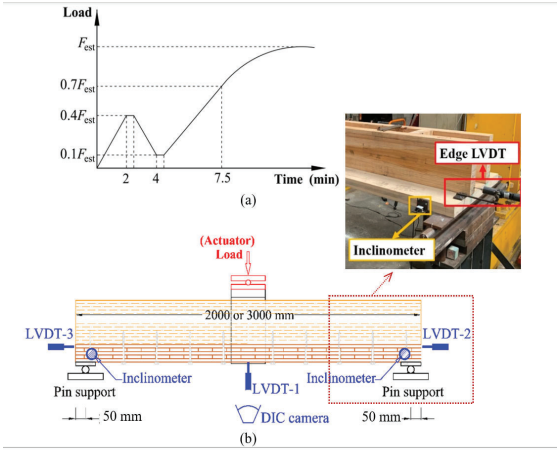

Figure 3: *(a) Loading procedure as per EN26891 [14] (b) loading and instrumentation of TTC subassembly.*

3.2 TTC subassemblies outline

Thirty-one TTC and six bare LVL or GLT beams representing the end span regions of a continuous timber/TTC floor (**Figure 4**) were fabricated and tested under hogging moment. The TTC and bare timber beams were either 2.0 m or 3.0 m long, which represent continuous TTC floors with span length in the range of L = 8-10 m, based on the assumption that the points of contraflexure are approximately located at cross-sections 0.125-0.15L away from the supporting columns. The TTC composites were benchmarked against the subassemblies with bare timber beams to determine contribution of the CLT slabs to the hogging moment and stiffness of the TTC beams/floors continuous across the columns.

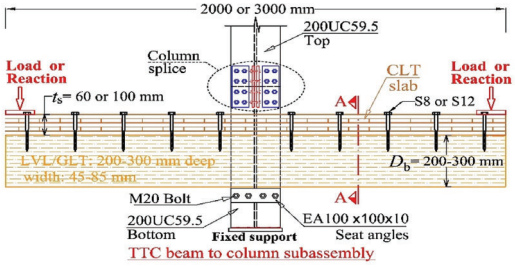

Figure 4: *TTC subassembly layout.*

Table 3: *Details of TTC specimen*

No.	Joists		Screw/Shear connector	Slab width (mm)	CLT Thickness (mm)	CLT orientation	Hole
	Size (mm)	Type/ Grade					
2 m long - Short span or group S							
S1 (No. 1)	200×65	LVL	KOP8	800	100	L	N
S1 (No. 2)	200×65	LVL	KOP8	800	100	L	N
S2	200×65	LVL	KOP12	800	100	L	N
S3	200×65	LVL	KOP12	800	60	L	N
S4 (No. 1)	300×45	LVL	KOP8	800	60	L	N
S4 (No. 2)	300×45	LVL	KOP8	800	60	L	N
S5	300×45	LVL	KOP8 + Glue	800	60	L	N
S6	295×85	GLT	KOP12	800	100	L	N
S7	295×85	GLT	KOP12	1000	100	L	N
S8 (No. 1)	200×65	LVL	KOP12	800	60	L	Y
S8 (No. 2)	200×65	LVL	KOP12	800	60	L	Y
S9 (No. 1)	300×45	LVL	KOP8	800	60	L	Y
S9 (No. 2)	300×45	LVL	KOP8	800	60	L	Y
S10 (No. 1)	295×85	GLT	KOP12	1000	100	L	Y
S10 (No. 2)	295×85	GLT	KOP12	1000	100	L	Y
S11	295×85	GLT	KOP12	800	100	L	Y
S12 (No. 1)	200×65	LVL	KOP12	800	60	C	Y
S12 (No. 2)	200×65	LVL	KOP12	800	60	C	Y
S13	295×85	GLT	KOP12	800	100	C	Y
3 m long - Long span or group L							
L1	295×85	GLT	KOP12	800	60	L	N
L2	295×85	GLT	KOP12	800	60	C	N
L3 (No. 1)	300×45	LVL	KOP8	800	60	L	Y
L3 (No. 2)	300×45	LVL	KOP8	800	60	L	Y
L4 (No. 1)	300×45	LVL	KOP8	800	60	C	Y
L4 (No. 2)	300×45	LVL	KOP8	800	60	C	Y
L5 (No. 1)	300×45	LVL	KOP8 + Glue	800	60	L	Y
L5 (No. 2)	300×45	LVL	KOP8 + Glue	800	60	L	Y
L6 (No. 1)	200×75	LVL	KOP8	800	100	C	Y
L6 (No. 2)	200×75	LVL	KOP8	800	100	C	Y
L7 (No. 1)	200×75	LVL	KOP12	800	100	C	Y
L7 (No. 2)	200×75	LVL	KOP12	800	100	C	Y

3.3 MODES OF FAILURE

In total, seven distinctive failure modes, i.e., I to VII, including six primary (I-VI) and one secondary (VII) were observed in the tested specimens. Failure mode I was associated with the onset of tensile flexural cracks (fracture) in the outermost lamella of the CLT panels. Failure modes II and III were observed in TTC beams with CLT panels loaded crosswise (i.e., perpendicular to the outer lamellae of the CLT). In mode II, fracture of the lamella along the edge of the glue line and in mode III, tensile fracture (perpendicular to the grain) took place. Failure mode IV was observed in CLT slabs loaded lengthwise and it was associated with rolling shear failure in the second lamella, which was loaded perpendicular to the grain.

Failure mode V was associated with the fracture of the epoxy line at the interface between the CLT and LVL beam when the composite action between the slab and the beam was developed by the combination of the screw and epoxy. Mode VI was associated with the onset of tensile flexural cracks in the LVL/GLT beams, and in mode VII shear cracks developed along the LVL/GLT beams and reached the end of the beam well into the post-peak (softening) stage. Mode VI predominantly took place in conjunction with Modes I-III while mode VII was mostly observed in 2 m long TTC beams. In all specimens (except for S6, S7 and S10), failure mode VII was a secondary mode that occurred after the onset of a primary mode and during the post-peak stage of the behaviour. In specimens S6, S7 and S10, mode VII was the dominant (primary)

failure mode that took place before others. The longitudinal shear cracks (in mode VII) mostly propagated along the glue line of the GLT beams and the shear cracks were at the height where the screw tips were located. This resulted in the tip of the screw to slightly bend.

Table 4: *Peak load, bending moment capacity, service stiffness and failure modes of the TTC specimens.*

No.	Peak load	Mean values			Failure modes
	F_{peak} (kN)	Bending capacity M_{peak} (kNm)	Stiffness $K_{s,0.4}$ (kN/mm)	Peak load F_{peak} (kN)	
2 m long - Short span or group S					
S1 (No. 1)	211.7	100.1 [89.1][1]	11.3	210.9 (0.6%)[2]	I, IV, VI
S1 (No. 2)	210.0				
S2	252	119.7 [106.5]	13.3	252	
S3	170.6	81.1 [72.1]	9.5	170.6	
S4 (No. 1)	198.4	96.3 [85.7]	15.7	202.7 (3.0%)	I, VI & VII
S4 (No. 2)	206.9				
S5	206.5	98.1 [87.3]	21.0	206.5	I, IV, V, VI, VII
S6	397.1	188.6 [167.8]	32.9	397.1	I, IV, VI, VII
S7	428.4	203.5 [181]	34.3	428.4	
S8 (No. 1)	159.0	74.6 [66.4]	8.7	157.1 (1.7%)	I, IV, VI
S8 (No. 2)	155.2				
S9 (No. 1)	202.7	94.4 [83.9]	14.7	198.6 (2.9%)	I, IV, VI
S9 (No. 2)	194.6				
S10 (No. 1)	386.0	197.3 [175.5]	34.0	415.4 (10%)	I, IV, VI, VII
S10 (No. 2)	444.7				
S11	384.8	182.8 [162.6]	33.7	384.8	
S12 (No. 1)	143.7	67.1 [59.7]	8.2	141.2 (2.5%)	II & VI
S12 (No. 2)	138.7				
S13	370.3	175.9 [156.5]	28.1	370.3	II, III, VI, VII
3 m long - Long span or group L					
L1	282.8	205.0 [190.2]	11.3	282.8	I & VI
L2	239.8	173.9 [161.3]	10.1	239.8	II, III, VI
L3 (No. 1)	138.5	108.1 [100.2]	5.8	149.1 (10%)	I, IV, VI
L3 (No. 2)	159.6				
L4 (No. 1)	126.9	90.1 [83.6]	5.0	124.3 (3%)	II, III, VI
L4 (No. 2)	121.7				
L5 (No. 1)	176.2	136.7 [126.8]	10.4	188.6 (9.3%)	I, IV, V & VI
L5 (No. 2)	201.1				
L6 (No. 1)	99.5	73.7 [68.3]	3.1	101.7 (3.1%)	II, III, IV & VI
L6 (No. 2)	103.8				
L7 (No. 1)	130.9	90.8 [84.2]	3.4	125.2 (6.4%)	II, III, IV & VI
L7 (No. 2)	119.5				

The load versus deflection evolution for specimens with 2 m and 3 m long TTC beams are plotted in Figure 5 and Figure 6, respectively. The mean peak load F_{peak} and the serviceability stiffness $K_{s,0.4}$ of the TTC specimens obtained from the load versus deflection results are summarised in Table 4. The service stiffness was taken as the slope of the line between the two points corresponding to $0.1F_{peak}$ and $0.4F_{peak}$ [14] on the load-deflection diagram.

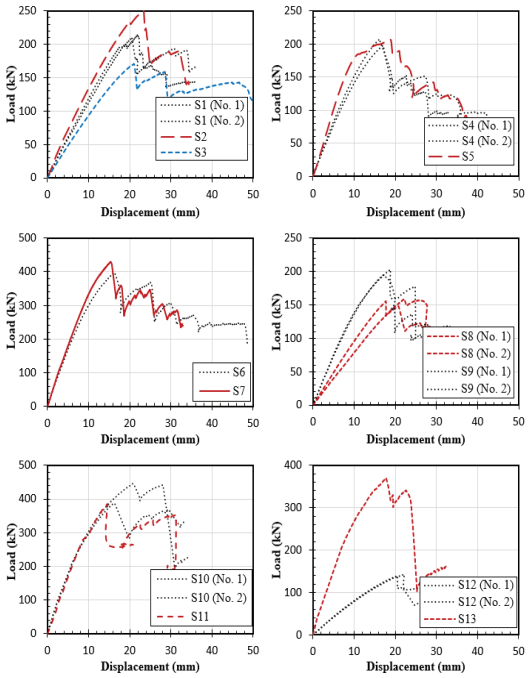

Figure 5 *Load versus deflection of the TTC subassemblies (group S, 2 m long TTC beams)*

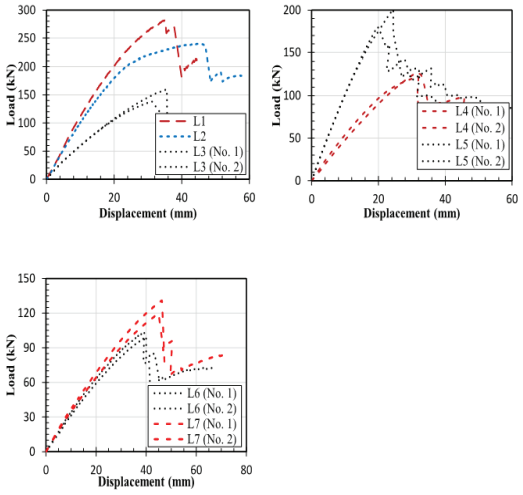

Figure 6 *Load versus deflection of the TTC subassemblies (group L, 3 m long TTC beams).*

3.4 EFFECT OF VARIOUS PARAMETERS

The width of the CLT slab and column penetration in the slab (resulting in the reduction of the slab area of up to 20%) had minor (less than 9%) influence on the stiffness and peak load. However, the CLT slab thickness (in the range of 60-100 mm) had a major (up to 48%) influence on the peak load and stiffness of the TTC beam subject to hogging moment. The size of shear connectors (degree of shear connection provided by 8-12 mm screws) and

https://doi.org/10.52202/069179-0008

orientation of the CLT slab had a moderate (max. 18-23%) influence on the load carrying capacity and stiffness of the samples. In the tested specimens, the stiffness and peak load of TTC specimens with lengthwise loaded CLT were up to 20% higher than the ones with CLT loaded crosswise.

3.5 ANALYTICAL RESULTS

The analytical model obtained from the solution to the Timoshenko composite beam was slightly more accurate than the *g*-method, especially for TTC beams with smaller shear span over cross-section depth ratio. But the *g*-method (EN 1995-1-1 [15]) is simpler, and more efficient and usable than the Timoshenko composite beam model. The comparison bar chart is shown in Figure 7.

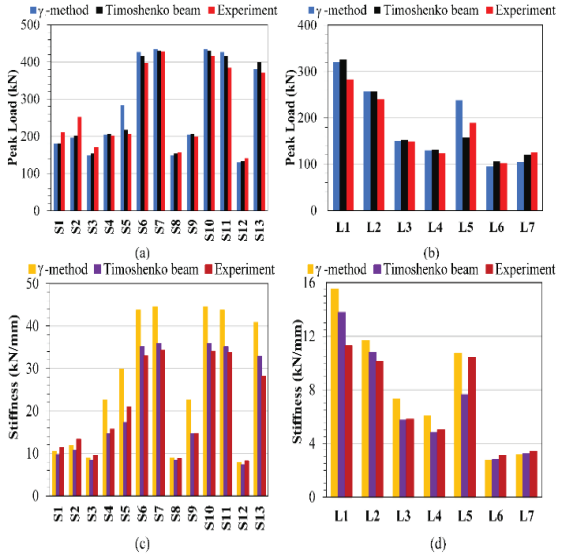

***Figure** 7 Comparison of (a-b) peak loads and (c-d) service stiffness values obtained from two analytical models and experimental results.*

For all specimens (except S5 and L5 with glued shear connections), the peak load analytically predicted by γ-method and Timoshenko beam model had close correlation with the experimental results. In the case of specimens S5 and L5, the gamma-method overestimated the peak load by 37.1% and 26.1%, respectively. The maximum difference between the peak load predicted by the Timoshenko beam model and the experimental peak load was less than 19.5% (observed in specimen S2). The service stiffness of the specimens (specially the S group with large cross-section depth over shear span ratio) predicted by the Timoshenko beam model was more accurate than the stiffness obtained from the γ-method as evident from the bar charts shown in Figure 7c-d.

4 FINITE ELEMENT MODELLING (FEM)

4.1 OVERVIEW

In the FE models, CLT panels were modelled using the layer-wise approach with mechanical properties assigned to parallel and perpendicular to the grain lamellae. However, the veneers and the lumbers in the LVL and GLT were not explicitly modelled, and LVL and GLT were treated as a single piece of timber. To enhance the computational efficiency and avoid numerical convergence/instability issues associated with stress concentration and fine meshes around the screw shear connectors, the shear connectors were modelled using nonlinear springs defined at the interface between slab and timber joists/beams. Apart from nonlinearities of steel, timber and concrete/grout, the geometrical non-linearity was also considered in the FE simulation, though effect of geometrical nonlinearity was deemed to be negligible.

The configuration and details of loading, boundary conditions and geometric outline of the TTC and TCC specimens modelled in ABAQUS are provided in Figure 8. To simplify the structure and increase speed of analyses without comprising the accuracy of the results, the steel column of the subassemblies was not modelled in the FE simulations. The load was applied to a stiff loading plate with a displacement rate consistent with the experiments. The supports of the timber composite beams were treated as an ideal pin and only the displacements in x, y, and z direction were fixed along the bottom centreline of the support plates accordingly (Figure 8). To prevent localised crushing and excessive deformation of the timber joists (loaded perpendicular to the grain), timber stiffeners were modelled underneath the loading plates (Figure 8). The stiffeners were assumed to be linear elastic materials with mechanical properties identical to timber joists/beams.

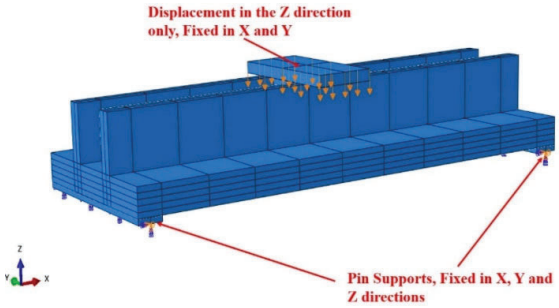

***Figure 8** Outline of the geometry, loading and support conditions considered in the FE model of TTC and TCC beams.*

4.2 MESH SIZE

The element used for modelling LVL, GLT, CLT, concrete slab, steel loading plate and support plates was a standard linear Hexagonal C3D8R (an 8-node linear brick) element with reduced integration and enhanced hour-glass control. The screws were modelled using a wedge 8-node linear brick (C3D8) element with full integration. The size and configuration of the FE mesh for the timber beams/slabs and screws are depicted in Figure 9 and the element size for each component is given in Table 5.

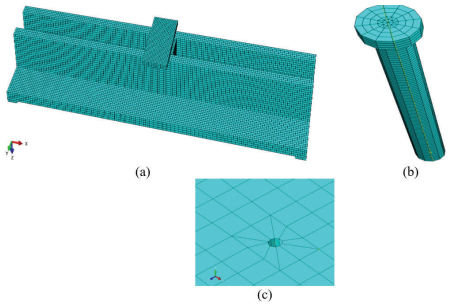

Figure 9 *FE mesh (a) entire TTC/TCC domain, (b) dowel and (c) domain around the hole.*

Table 5 *Mesh type and size for each respective element used in the TTC model.*

Structural component	Mesh type	Mesh size
CLT Slab	C3D8R	15
LVL	C3D8R	15
GLT	C3D8R	15
Stiffeners	C3D8R	15
Steel Load Plate	C3D8R	15
Steel Support plates	C3D8R	15
Dowel (KOP8 and KOP12 screws)	C3D8R	2

4.3 COMPARISON AND DISCREPANCIES

The FEM was adequately able to capture the results within close proximity. There was a slight discrepancy between the experimental GLT members and the FEM GLT. This can be attributed to rolling shear failure and stress localisation. Furthermore, some specimen was modelled with screws instead of line connectors. The results are summarised in Figure 10.

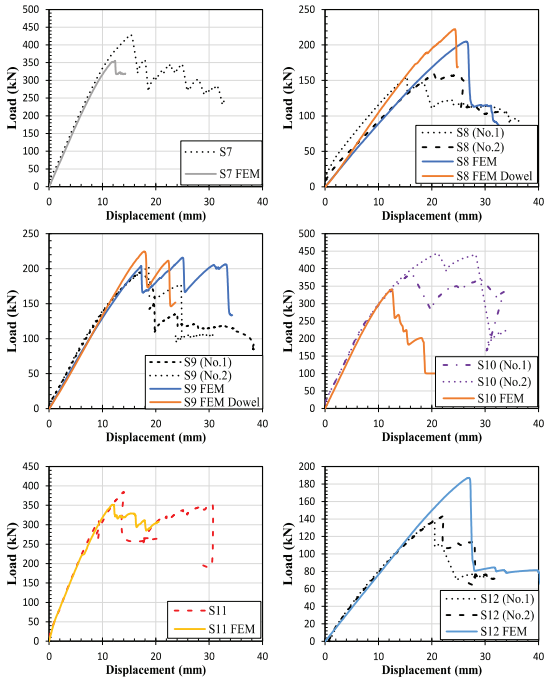

Figure 10 *experimental vs analytical Load vs displacement with line connectors and dowels.*

5 CONCLUSIONS

The purpose of this project was to investigate the structural performance of TTC and TCC systems through full scale laboratory experimentation, advanced numerical simulation, and development of analytical models. Emphasis was placed on structural behaviour of the TTC and TCC floors subjected to hogging moment.

- The dominant failure mode of TTC beams under hogging moment was brittle and it was associated with tensile flexural failure in the outermost lamellae of the CLT slabs combined with tensile flexural failure in the LVL/GLT joists. These modes were followed by rolling shear in the CLT slab, or shear failure of the LVL/GLT joists specially during the post-peak stage of the behaviour.
- The orientation of CLT slabs had some effect on the stiffness and load carrying capacity. In the tested specimens, the stiffness and peak load of TTC specimens with lengthwise loaded CLT were up to 20% higher than the ones with CLT loaded crosswise.
- Despite a 20% reduction in the cross-sectional area of the CLT slabs, because of the column penetration, the reduction in the stiffness and load carrying capacity was less than 9%.
- The size of screw shear connectors (8 and 12 mm) had a moderate (up to 18%) influence on the peak load and stiffness of the TTC under hogging moment. However, using the epoxy glue in conjunction with screws considerably increased stiffness of the TTC specimens. The joists glued to the CLT slabs with opening also prevented the crack initiation and propagation from

https://doi.org/10.52202/069179-0008

the corner of the penetration/opening and increased the peak load of the TTC accordingly.

- The analytical model obtained from the solution to the Timoshenko composite beam was slightly more accurate than the γ-method, especially for TTC beams with smaller shear span over cross-section depth ratio. But the γ-method is simpler, and more efficient and usable than the Timoshenko composite beam model.
- The nonlinear 3D FE models were able to capture the complex (combination of shear, tension parallel and perpendicular to the grain) failure modes of TTC and TCC beam to column subassemblies. Small difference was found between the results of two modelling strategies, i.e., explicit modelling of the screw shear connectors and implicit modelling of the she connectors with nonlinear springs/links.

ACKNOWLEDGEMENT

The Authors would like to thank UNSW Heavy Structure Lab (HSL) team for their efforts during the fabrication process of project.

REFERENCES

[1] Hammad, M., H. Valipour, and M. Bradford, *Timber-timber composite (TTC) beams subjected to hogging moment.* Construction and Building Materials, 2021. **321**.

[2] Woodard, A.C. and H.R. Milner, *Sustainability of timber and wood in construction*, in *Sustainability of Construction Materials*. 2016. p. 129-157.

[3] Milner, H.R. and A.C. Woodard, *Sustainability of engineered wood products*, in *Sustainability of Construction Materials*. 2016. p. 159-180.

[4] Gharib, M., et al., *Three-dimensional constitutive modelling of arbitrarily orientated timber based on continuum damage mechanics.* Finite Elements in Analysis and Design, 2017. 135: p. 79-90.

[5] *Standards Australia Limited, AS 1720.1-2010 Timber structures - Design methods*. 2010.

[6] British Standard, I., *BS EN 408:2010+A1:2012: Timber structures - Structural timber and glued laminated timber - Determination of some physical and mechanical properties.* BSI Standards Publication, 2012.

[7] *AS/NZ1328 (1998), Glued laminated structural timber Part 1: Performance requirements and minimum production requirements.* 1998.

[8] Zealand, S.A.o.A.a.S.N., *AS_NZS 4357.0_2005 Structural laminated veneer lumber - Specifications*. 2005.

[9] *Standards Association of Australia and Standards New Zealand, AS NZS 1080.1 2012 Timber Methods of test - Moisture content*. 2012.

[10] Milner, H.R., *Design Values for Australian Glulam*, F.W.P.R.D. Corporation, Editor. 2004: Australia.

[11] Standard, I., *EN 14592 Timber structures-Dowel-type fasteners-Requirements*. 2012.

[12] Blass, H.J. and C. Sandhaas, *Timber Engineering Principles for Design*. 2017, KIT Scientific Publishing.

[13] *AS/NZS 10984.1 Timber structures — Dowel-type fasteners Part 1 : Determination of yield moment.* 2015.

[14] *EN 26891:1991- Timber Structures - Joints made with mechanical fasteners - General principles for The determination of strength and deformation characteristics*. 2001. 43-43.

[15] Standards, B., *Eurocode 5 (EC 5), Design of timber structures- Part 1-1: General- Common rules and rules for buildings. BS EN 1995-1-1*. 2004, British Standards.